λ-Jellium Model for the Anomalous Hall Crystal

Tomohiro Soejima (副島智大),[1,*] Junkai Dong (董焌锴),[1,2,*] Ashvin Vishwanath,[1] and Daniel E. Parker[3]
[1]Department of Physics, Harvard University, Cambridge, Massachusetts 02138, USA
[2]Kavli Institute for Theoretical Physics, University of California, Santa Barbara, California 93106, USA
[3]Department of Physics, University of California at San Diego, La Jolla, California 92093, USA

(Received 28 May 2025; accepted 23 September 2025; published 30 October 2025)

The jellium model is a paradigmatic problem in condensed matter physics, exhibiting a phase transition between metallic and Wigner crystal phases. However, its vanishing Berry curvature makes it ill suited for studying recent experimental platforms that combine strong interactions with nontrivial quantum geometry. These experiments inspired the anomalous Hall crystal (AHC)—a topological variant of the Wigner crystal. The AHC spontaneously breaks continuous translation symmetry but has a nonzero Chern number. In this Letter, we introduce λ-jellium, a minimal extension of the two-dimensional jellium model. Its Berry curvature distribution is controlled by a single parameter λ, where $\lambda = 0$ corresponds to the standard jellium model. This setup facilitates the systematic exploration of Berry curvature's impact on electron crystallization. The phase diagram of this model, established using self-consistent Hartree Fock calculations, reveals several interesting features: (i) The AHC phase occupies a large region of the phase diagram. (ii) Two distinct Wigner crystal phases, the latter enabled by quantum geometry, and two distinct Fermi liquid phases are present. (iii) A continuous phase transition separates the AHC and one of the Wigner crystal phases. (iv) In some parts of the AHC phase, the lattice geometry is nontriangular, unlike in the classical Wigner crystal. In addition to elucidating the physics of correlated electrons with nonzero Berry curvature, we expect that the simplicity of the model makes it an excellent starting point for more advanced numerical methods.

DOI: 10.1103/x53d-12s6

In the classic problem considered by Wigner [1], electron crystallization driven by strong Coulomb interactions was examined within the jellium model, in which an electron fluid embedded in a uniform neutralizing background spontaneously breaks translation symmetry upon decreasing the density. The two-dimensional incarnation of the jellium model, the two-dimensional electron gas (2DEG), has since been studied extensively using advanced numerical techniques [2–13], which revealed the importance of beyond-mean-field effects for the energy competition of the Wigner crystal (WC) phase with the Fermi liquid.

Recent experiments [14–18] in rhombohedral multilayer graphene (RMG), where new phases including integer and fractional quantum Hall phases emerge at low electronic densities and zero magnetic field, have inspired an explosion of theoretical interest in topological crystalline phases of matter. We, along with our collaborators and another simultaneous work, proposed [19,20] the possibility of an interaction-driven Chern insulator that spontaneously breaks continuous translation symmetry, which we dubbed the anomalous Hall crystal (AHC).

The complexity of the microscopic RMG Hamiltonian, consisting of ten orbitals and a morass of single-particle hopping parameters, makes it difficult to distill simple physics, preventing a unified understanding despite intensive efforts [21–29]. This has led to a flurry of interest in simplified models for AHCs [30–32]. However, these models either are phenomenological mean-field models or contain a large number of spinor components, thus precluding the possibility of beyond-mean-field numerics. Indeed, determining the fate of the AHC in the presence of beyond-mean-field quantum fluctuations is an urgent challenge.

To understand the universal physics of topological band minima, eventually including quantum fluctuations, one should consider the simplest possible model. To this end, we propose λ-jellium. This two-band model endows the quadratic dispersion of the jellium model with a nontrivial skyrmionic texture in momentum space, which is responsible for its nonzero Berry curvature. The model contains two tuning parameters: r_s and λ. The familiar r_s is the ratio between the quadratic dispersion and Coulomb interaction terms, whereas $1/\lambda$ controls the extent of the skyrmionic texture. In the $\lambda \to 0$ limit, the model reduces to the standard two-dimensional jellium model, thus allowing us to systematically understand the effect of Berry curvature. Our model, given its simplicity, limited spinor dimensions, and connection to the jellium model, can be studied with beyond-mean-field techniques employed such

[*]These authors contributed equally to this work.

as variational and diffusion Monte Carlo methods developed over many decades [3–12].

To pave the way for these advanced methods, we perform extensive self-consistent Hartree-Fock (HF) calculations of the phase diagram of the λ-jellium model. We find that the AHC phase occupies a significant region of the phase diagram. In addition, we also find two distinct Wigner crystal phases: a conventional Wigner crystal and a "halo Wigner crystal" with distinct symmetry properties. Two Fermi liquids, whose Fermi surfaces are circular and annular, also appear in the phase diagram. We find that the halo Wigner crystal and the annular Fermi liquid arise due to the interplay between interactions and nontrivial quantum geometry. We further find a quantum critical point between the AHC phase and the halo Wigner crystal, which is described by an emergent Dirac cone.

Finally, we find that, in some parts of the AHC phase, spontaneous crystallization picks a nontriangular lattice geometry. This subtlety in the choice of lattice geometry already exists in the case of Wigner crystals, where the large r_s classical electrostatic limit selects the triangular lattice. However, deep in the quantum regime, the preferred lattice geometry is not *a priori* clear. For instance, with spinful electrons at small interaction strengths, a square antiferromagnet wins over the triangular lattice within HF [13]. Similarly, in λ-jellium we find that nontriangular AHC states can be energetically preferred over triangular AHC states. This echoes earlier works on RMG, which found unit cells with multiple electrons [17,27] or nontriangular unit cells [33] can be stabilized.

The λ-jellium model—We now introduce the Hamiltonian for λ-jellium, a two-band generalization of jellium with a skyrmionic texture in momentum space that provides a tunable amount of Berry curvature.

Recall that the Hamiltonian for the (spinless) 2DEG is [4]

$$\hat{H}_{\mathrm{2DEG}} = -\frac{1}{r_s^2}\sum_{i=1}^{N}\nabla_i^2 + \frac{2}{r_s}\sum_{i<j}^{N}\frac{1}{|\boldsymbol{r}_i - \boldsymbol{r}_j|}, \tag{1}$$

where length is measured in units of the typical interparticle distance a (defined below) and energy has units of Rydbergs Ry [34]. These are related to microscopic units by $r_s = (a/a_0)$, $a = (1/\sqrt{\pi\rho})$, $a_0 = [\hbar^2/(me^2)]$, and $\mathrm{Ry} = [(me^4)/(2\hbar^2)]$ [4]. Here, ρ is the number density of electrons, a circle of radius a encloses one particle on average, and r_s is the dimensionless potential or kinetic ratio. This choice sets the Fermi momentum to be $2/a$, which means $k_F = 2$ in the unit system used in Eq. (1).

We now present a *local* two-band generalization of this model whose lower band has identical dispersion and interaction to Eq. (1) but includes a tunable amount of Berry curvature concentrated at the band minimum. To maintain locality, we use a kinetic energy that is a simple polynomial in the derivative operators:

$$\hat{h} = \Delta\begin{bmatrix} -\lambda^2\nabla^2 & i\lambda\partial \\ i\lambda\bar{\partial} & 1 \end{bmatrix}, \tag{2}$$

where $\partial = \partial_x - i\partial_y$, $\nabla^2 = \partial_x^2 + \partial_y^2$, and Δ is a large and positive constant.

One can think of this as a Dirac equation with a momentum-dependent mass (see Supplemental Material [35]). The lower band of $\hat{h}$ is exactly flat: $\epsilon_{\boldsymbol{q}} = 0$. Its wave function is $\phi(\boldsymbol{r}) = (1/\sqrt{A})\int d^2\boldsymbol{q}\phi_{\boldsymbol{q}}e^{i\boldsymbol{q}\cdot\boldsymbol{r}}$ with spinor

$$\phi_{\boldsymbol{q}} = \frac{1}{\sqrt{1+\lambda^2 q^2}}\begin{bmatrix} 1 \\ \lambda(q_x + iq_y) \end{bmatrix}, \tag{3}$$

where $q = |\boldsymbol{q}|$. The upper band is separated by a gap with minimum size Δ. Henceforth, we take $\Delta \to \infty$ and focus on the lower band.

We now study interacting electrons in the nontrivial lower band Eq. (3). To do so, we combine Eqs. (1) and (2) to form the full model, which we call λ-jellium:

$$\hat{H} = \Delta\sum_{i=1}^{N}\begin{bmatrix} -\lambda^2\nabla_i^2 & i\lambda\partial_i \\ i\lambda\bar{\partial}_i & 1 \end{bmatrix} - \sum_{i=1}^{N}\hat{I}_2\frac{\nabla_i^2}{r_s^2} + \frac{2}{r_s}\sum_{i<j}^{N}\frac{1}{|\boldsymbol{r}_i - \boldsymbol{r}_j|}, \tag{4}$$

where $\hat{I}_2$ is the identity in spinor space and the interaction is spinor isotropic. We fix the number density to be ρ, using the same parametrization as in the standard 2DEG. This Hamiltonian is controlled by two dimensionless parameters: the familiar potential or kinetic ratio r_s and a new parameter λ that controls the concentration of Berry curvature in the lower band. We note that the single-particle part of this model can be obtained as a particular parameter choice of the two-band model discussed in Ref. [41]. The same Hamiltonian, up to a choice of the diagonal term, was written down in Refs. [31,42].

Single-particle properties—Let us set out the single-particle properties of λ-jellium. In addition to continuous translation symmetry, the Hamiltonian has U(1) rotation symmetry $\hat{R}_\theta\phi(\boldsymbol{r}) = \mathrm{diag}[1, e^{i\theta}]\phi(R_{-\theta}\boldsymbol{r})$, where the diagonal matrix acts in spinor space. Its single-particle energy is $\epsilon_{\boldsymbol{q}} = (q^2/r_s^2)$ in the lower band, matching the 2DEG. The nontrivial spinor $\phi_{\boldsymbol{q}}$ gives the lower band a skyrmionic texture in momentum space, with a spin-up "skyrmion core" near $\boldsymbol{q} = 0$ and spin down at infinity. It wraps the Bloch sphere exactly once as $\boldsymbol{q}$ varies, producing Berry curvature $\Omega(\boldsymbol{q}) = 2[\lambda/(\lambda^2|\boldsymbol{q}|^2 + 1)]^2$ [Fig. 1(b)] [43]. Within a disk of radius κ, the enclosed Berry curvature is a Lorentzian $I(\kappa) = 2\pi[(\lambda^2\kappa^2)/(1+\lambda^2\kappa^2)]$, with which takes half the maximal value at $\kappa = 1/\lambda$. As λ grows, the total Berry curvature is always 2π but becomes concentrated at $\boldsymbol{q} = 0$, reaching $I(k_F = 2) = \pi$ at $\lambda = \frac{1}{2}$. The Berry curvature vanishes when $\lambda = 0$, whereupon the lower band

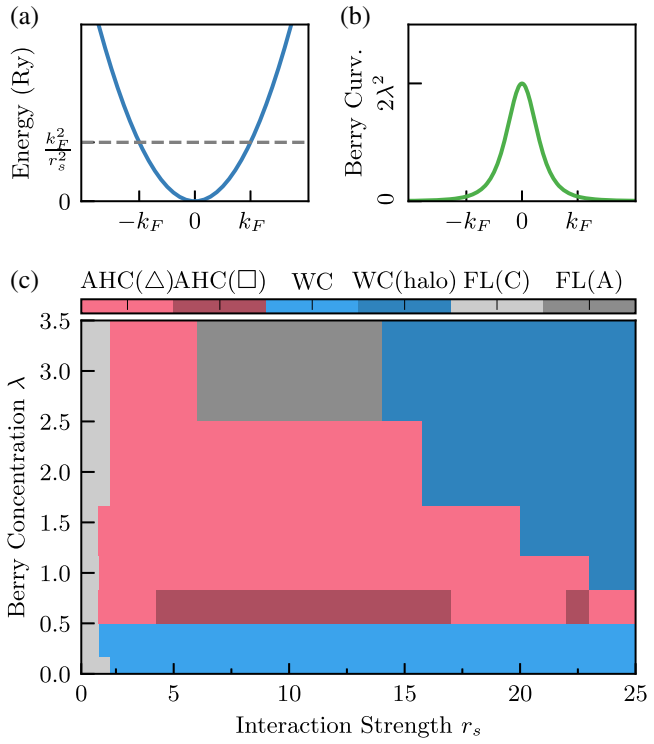

FIG. 1. (a) Quadratic dispersion and (b) Berry curvature of the lower single-particle band of the topological electron gas model, Eq. (4). (c) Mean-field phase diagram. The limit $\lambda = 0$ is identical to the spinless 2DEG. Two significant Fermi liquid (FL) regions are present: one at low interaction strengths and one at large interaction strength and Berry curvature concentration. Under strong interactions, a WC appears that undergoes a first-order transition to an AHC at $\lambda \approx \frac{1}{2}$. A putative second-order transition back to a WC appears at larger λ. A significant region of AHC is present, with the competition between triangular and square AHCs shown by light pink [AHC(△)] when the triangular AHC has lower energy than the square and dark pink [AHC(□)] when the reverse is true. Within the AHC phase, a square unit cell is preferred to a triangular unit cell in a region near $\lambda = 2/3$.

of $\hat{H}$ reduces to the spinless 2DEG. λ-jellium, therefore, provides a minimal modification to the standard 2DEG whose interaction strength and band topology can be tuned continuously and independently. The unnormalized spinors $\sqrt{1+\lambda^2 q^2}\phi_{\boldsymbol{q}}$ are holomorphic with respect to $\boldsymbol{q}$, giving the lower band of λ-jellium "ideal quantum geometry" [44,45].

Mean-field phase diagram—We now study the phase diagram of λ-jellium, where we find a Berry-curvature-induced anomalous Hall crystal competing with other crystalline phases and liquids. We work at mean-field level, employing self-consistent Hartree-Fock with three possible translation patterns imposed: (I) continuous translation symmetry (CTS), (II) a discrete translation symmetry (DTS) with a triangular lattice with one electron per unit cell, and (III) DTS with a *square* lattice with on electron per unit cell. The calculation with CTS is performed in the thermodynamic limit, while the DTS calculation is done on

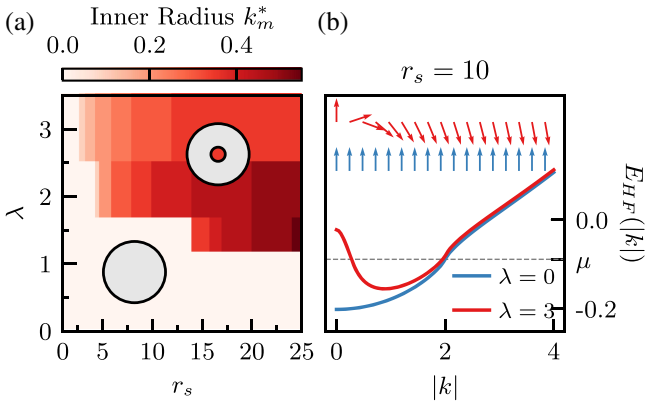

FIG. 2. Fermi liquid phases of λ-jellium assuming continuous translation symmetry. (a) Self-consistent inner radius k_m^* of the Fermi surface. (b) The Fermi liquid develops a strong peak at $\boldsymbol{k} = 0$ at large λ, r_s due to exchange (Fock) interactions, leading to annular Fermi surfaces. Arrows show the pseudospin on the Bloch sphere, $(\langle\sigma_x\rangle, \langle\sigma_z\rangle)$ along the k_x axis. A localized skyrmion core is present at $\lambda = 3$.

$N_k \times N_k$ unit cells, with N_k going up to 36. See Supplemental Material [35] for numerical details. The resulting phase diagram is shown in Fig. 1(c). We now embark on a tour of the phase diagram.

Circular and annular Fermi liquids—The phase diagram [Fig. 1(c)] supports two regions with distinct Fermi liquid ground states, whose energy competition is driven by nonuniform quantum geometry. To understand the competition between the Fermi liquids, we analyze the phase diagram while imposing continuous translation symmetry. The mean-field states are entirely characterized by their momentum space occupations $n(\boldsymbol{k}) = \langle c_{\boldsymbol{k}}^\dagger c_{\boldsymbol{k}}\rangle$ with *unbounded* momentum $\boldsymbol{k}$. At small λ, we find the textbook circular Fermi liquid, with $n(\boldsymbol{k}) = \theta(|\boldsymbol{k}| - k_F)$. At moderate interaction strengths, λ drives a transition to an annular Fermi liquid. This phase has two concentric circular Fermi surfaces, so that $n(\boldsymbol{k}) = 1$ when $k_m \le |\boldsymbol{k}| \le k_M$ and otherwise vanishes. The competition between the circular and annular Fermi liquids, which we call FL(C) and FL(A), respectively, is shown in Fig. 2(a).

Interactions drive the formation of the annular Fermi liquid via a mechanism that can be understood qualitatively from the skyrmionic spinor texture. This arises from the Hartree-Fock band structure [35]

$$E_{\mathrm{HF}}(\boldsymbol{k}) = \frac{|\boldsymbol{k}|^2}{r_s^2} - \frac{1}{A}\sum_{\boldsymbol{q}} V_{\boldsymbol{q}} |\Lambda_{\boldsymbol{q}}(\boldsymbol{k})|^2 n(\boldsymbol{k}+\boldsymbol{q}), \qquad (5)$$

where the sum runs over unrestricted momenta, $V_{\boldsymbol{q}} = 2\pi/q$, and $\Lambda_{\boldsymbol{q}}(\boldsymbol{k}) = \phi_{\boldsymbol{k}+\boldsymbol{q}}^\dagger \phi_{\boldsymbol{k}}$ is the form factor. A nontrivial form factor $|\Lambda| < 1$ reduces the exchange energy gain from the Fock term, which favors ferromagnetic spinor configuration. How does this work with the skyrmionic spinor texture Eq. (3)? For small λ, the skyrmion core

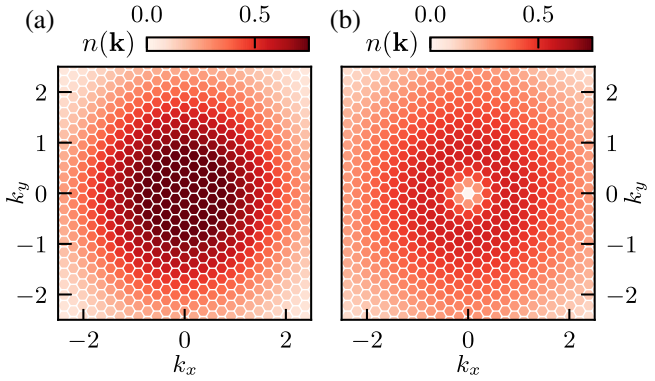

FIG. 3. Occupations of plane wave states in the lower band for different Wigner crystals. (a) Normal Wigner crystal at $(r_s, \lambda) = (20, 0)$. (b) Halo Wigner crystal at $(r_s, \lambda) = (20, 2.5)$. The $\boldsymbol{k} = 0$ region is depleted due to the Fock interactions at large λ.

region where spins point up is large compared to k_F. The form factors are, therefore, close to unity, giving a large negative exchange energy [Fig. 2(b)]. Conversely, large λ spinors have a small skyrmion core compared to k_F, with most states inside the noninteracting Fermi surface pointing down. Occupying the misaligned spinors near the core incurs a significant energy penalty. This drives the state to deplete the skyrmion core, resulting in an annular Fermi surface [Fig. 2(a)]. The depletion of $\boldsymbol{k} = 0$ will be a recurring feature throughout the phase diagram.

Halo Wigner crystals—Wigner crystal phases are characterized by spontaneous breaking of continuous symmetry that produces an insulator with zero Chern number. The 2DEG is known to host triangular Wigner crystalline states at large r_s [46–48]. Mean-field calculations underestimate the value of critical r_s between ferromagnetic FL and WC to be around 2 [13]. The λ-jellium model phase diagram, which is continuously connected to 2DEG in the $\lambda \to 0$ limit, also hosts Wigner crystalline phases, shown in Fig. 1(c).

At large r_s and λ, there is a distinct Wigner crystal phase—also with a triangular lattice—which we call a halo Wigner crystal. A similar crystalline phase was recently studied in Bernal bilayer graphene [36]. To see this, we plot the momentum space occupation number $n(\boldsymbol{k}) = \langle c^\dagger_{\boldsymbol{k}} c_{\boldsymbol{k}} \rangle$ for a normal Wigner crystal and a halo Wigner crystal in Figs. 3(a) and 3(b). We see that $n(\boldsymbol{k} = 0)$ takes the maximal value for the normal Wigner crystal, while $n(\boldsymbol{k} = 0) = 0$ for the halo Wigner crystal.

The vanishing of $n(\boldsymbol{k} = 0)$ is, in fact, enforced by how the crystal transforms under C_3 symmetry. Thus, the orbitals occupied at the high-symmetry points must be eigenstates of the C_3 symmetry with a definite angular momentum. Concretely, the C_3 angular momentum is

$$\hat{C}_3 \Psi^{\mathrm{WC}}_\Gamma = \Psi^{\mathrm{WC}}_\Gamma, \qquad \hat{C}_3 \Psi^{\mathrm{halo\,WC}}_\Gamma = e^{i2\pi/3} \Psi^{\mathrm{halo\,WC}}_\Gamma, \quad (6)$$

where Ψ_Γ is the single-particle orbital at the Γ point. Since the angular momentum at Γ does not depend on the choice of C_3 centers, the halo Wigner crystal and the normal Wigner crystal are distinct crystalline insulators with different symmetry properties [49]. This transition can, in fact, be understood from a simple semiclassical analysis [36], as we review in [35].

Anomalous Hall crystal—Because of the coexistence of single-particle Berry curvature and a trend toward crystallization at large interactions, we expect the AHC—a crystalline phase that becomes a Chern insulator when pinned—to appear [24,25,30–32]. At moderate r_s, we indeed observe an AHC phase. The phase boundary from WC to AHC occurs around $\lambda = 1/2$, where the Berry curvature within the Fermi surface reaches π—consistent with the prediction of Ref. [25]. At large r_s, the interaction mixes the single-particle bands strongly, and the AHC is overtaken by the halo WC.

At even larger $\lambda \gtrsim 2.5$, the AHC undergoes a transition to the annular Fermi liquid. Finite-size effects are particularly acute in the large λ regime due to the tiny skyrmion core in momentum space.

Second-order topological phase transition—We now examine the crystal-to-crystal phase transitions in λ-jellium, shown in Fig. 1(c). The transitions between AHC to WC and WC to halo-WC are first order, as the charge gap remains finite across the transitions. The transition between halo WC and AHC, on the other hand, appears to be continuous, as the charge gap closes at the transition [Fig. 4(a)].

The origin of this continuous transition can be understood from the Hartree-Fock band structure in Figs. 4(c) and 4(d). There the bands are colored according to their spinor polarization $z_a(\boldsymbol{k}) = \langle \psi_{a\boldsymbol{p}} | \sigma_z | \psi_{a\boldsymbol{p}} \rangle$, where σ_z acts in spinor space and $|\psi_{a\boldsymbol{p}}\rangle$ is the Bloch state at $\boldsymbol{p}$ for band $a = 1, 2$, counting from below. The spinor polarization flips at the transition, signaling change in angular momentum. This is accompanied by a change in the sign of Berry curvature around the Γ point [Fig. 4(b)]. The vicinity of Γ is, therefore, well described by a massive Dirac model with mass inversion.

AHC lattice geometry—In the *classical* Wigner crystal $r_s \to \infty$, the triangular lattice is preferred over the square lattice by about 0.5% [46]. A square lattice, however, can be stabilized at small r_s [13]. The preference for a triangular lattice, therefore, depends on the specific details of the Wigner crystal phase.

Does the AHC prefer a triangular lattice? To understand this, we examine the energetic competition within the AHC phase between the triangular lattice and the square lattice. Our result, shown in Fig. 1(c), is that, while the triangular lattice is preferred over the square in most of the AHC phase diagram, the reverse is true near the phase boundary between normal WC and AHC. The energetic competition remains close, with the square lattice favored by <0.5% at

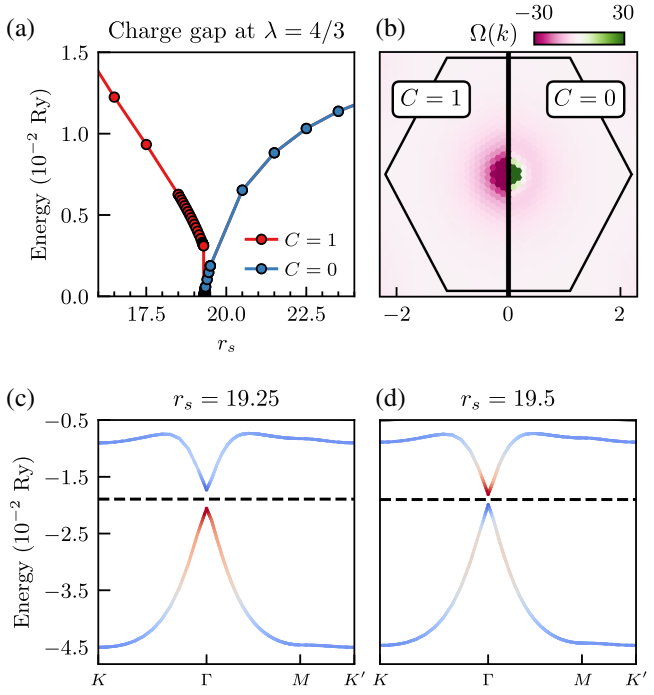

FIG. 4. Continuous phase transition driven by r_s at $\lambda = 4/3$. (a) Direct charge gap near the phase boundary between AHC and the halo WC. (b) The Berry curvature of an AHC ($r_s = 19.25$) and WC ($r_s = 19.5$) near the transition. It is strongly peaked around the Γ point, saturating the color scale. (c), (d) Self-consistent Hartree-Fock band structures before and after the transitions. Coloring corresponds to $z_a(\boldsymbol{p})$, with red corresponding to occupying the first component. Clearly, the r_s tuned transition corresponds to a band inversion transition.

most for $\lambda = 2/3$. In contrast, the triangular lattice is more stable at larger λ and r_s. We caution that another unit cell shape may have yet-lower energy in this region; future work will examine the full landscape of possible unit cells [50].

Discussion—This Letter studied λ-jellium, a minimal extension of jellium with topological crystalline phases including an anomalous Hall crystal. Its phase diagram captures the key features of more complex microscopic models [19–23,31] at mean-field level, suggesting universality in topological band minima.

A crucial next step is to move beyond mean-field techniques. As mentioned above, the two-component nature of our model together with the fact that only first and second derivatives appear make it well suited for a variety of many-body numerical techniques, including variational Monte Carlo and neural network wave function methods. λ-jellium may, therefore, be a good model to establish crystallization with a nontrivial Chern number at the many-body level.

Acknowledgments—We thank Ophelia Evelyn Sommer, Taige Wang, Tianle Wang, Mike Zaletel, Patrick Ledwith, and Eslam Khalaf for related collaborations and useful insights. We acknowledge Erez Berg, Yaar Vituri, Agnes Valenti, Miguel Morales, Paul Yang, Shiwei Zhang, Félix Desrochers, Yong Baek Kim, Adrian Po, and Trithep Devakul for fruitful discussions. This research was supported in part by grant NSF PHY-2309135 to the Kavli Institute for Theoretical Physics (KITP). This research is funded in part by the Gordon and Betty Moore Foundation's EPiQS Initiative, Grant No. GBMF8683 to T. S. A. V. and J. D. were funded by NSF DMR-2220703. D. E .P. acknowledges startup funds from UC San Diego. This work used the Expanse cluster at the San Diego Supercomputer Center through allocation PHY240272 from the Advanced Cyberinfrastructure Coordination Ecosystem: Services & Support (ACCESS) program, which is supported by U.S. National Science Foundation Grants No. 2138259, No. 2138286, No. 2138307, No. 2137603, and No. 2138296.

Data availability—The data that support the findings of this article are not publicly available upon publication because it is not technically feasible and/or the cost of preparing, depositing, and hosting the data would be prohibitive within the terms of this research project. The data are available from the authors upon reasonable request.

[1] E. Wigner, On the interaction of electrons in metals, Phys. Rev. **46**, 1002 (1934).
[2] Gabriele Giuliani and Giovanni Vignale, *Quantum Theory of the Electron Liquid* (Cambridge University Press, Cambridge, England, 2005).
[3] D. Ceperley, Ground state of the fermion one-component plasma: A Monte Carlo study in two and three dimensions, Phys. Rev. B **18**, 3126 (1978).
[4] B. Tanatar and David M. Ceperley, Ground state of the two-dimensional electron gas, Phys. Rev. B **39**, 5005 (1989).
[5] Paola Gori-Giorgi, Saverio Moroni, and Giovanni B. Bachelet, Pair-distribution functions of the two-dimensional electron gas, Phys. Rev. B **70**, 115102 (2004).
[6] S. De Palo, M. Botti, S. Moroni, and Gaetano Senatore, Effects of thickness on the spin susceptibility of the two dimensional electron gas, Phys. Rev. Lett. **94**, 226405 (2005).
[7] D. Varsano, S. Moroni, and G. Senatore, Spin-polarization transition in the two-dimensional electron gas, Europhys. Lett. **53**, 348 (2001).
[8] Claudio Attaccalite, Saverio Moroni, Paola Gori-Giorgi, and Giovanni B. Bachelet, Correlation energy and spin polarization in the 2d electron gas, Phys. Rev. Lett. **88**, 256601 (2002).
[9] Francesco Rapisarda and Gaetano Senatore, Diffusion Monte Carlo study of electrons in two-dimensional layers, Aust. J. Phys. **49**, 161 (1996).
[10] N. D. Drummond and R. J. Needs, Phase diagram of the low-density two-dimensional homogeneous electron gas, Phys. Rev. Lett. **102**, 126402 (2009).

[11] N. D. Drummond and R. J. Needs, Quantum Monte Carlo study of the ground state of the two-dimensional Fermi fluid, Phys. Rev. B **79**, 085414 (2009).
[12] Sam Azadi, N. D. Drummond, and S. M. Vinko, Quantum Monte Carlo study of the phase diagram of the two-dimensional uniform electron liquid, Phys. Rev. B **110**, 245145 (2024).
[13] J. R. Trail, M. D. Towler, and R. J. Needs, Unrestricted Hartree-Fock theory of Wigner crystals, Phys. Rev. B **68**, 045107 (2003).
[14] Zhengguang Lu, Tonghang Han, Yuxuan Yao, Aidan P Reddy, Jixiang Yang, Junseok Seo, Kenji Watanabe, Takashi Taniguchi, Liang Fu, and Long Ju, Fractional quantum anomalous Hall effect in multilayer graphene, Nature (London) **626**, 759 (2024).
[15] Jian Xie, Zihao Huo, Xin Lu, Zuo Feng, Zaizhe Zhang, Wenxuan Wang, Qiu Yang, Kenji Watanabe, Takashi Taniguchi, Kaihui Liu, Zhida Song, X. C. Xie, Jianpeng Liu, and Xiaobo Lu, Tunable fractional Chern insulators in rhombohedral graphene superlattices, arXiv:2405.16944.
[16] Youngjoon Choi, Ysun Choi, Marco Valentini, Caitlin L. Patterson, Ludwig F. W. Holleis, Owen I. Sheekey, Hari Stoyanov, Xiang Cheng, Takashi Taniguchi, Kenji Watanabe, and Andrea F. Young, Electric field control of superconductivity and quantized anomalous Hall effects in rhombohedral tetralayer graphene, Nature (London) **639**, 342 (2025).
[17] Dacen Waters, Anna Okounkova, Ruiheng Su, Boran Zhou, Jiang Yao, Kenji Watanabe, Takashi Taniguchi, Xiaodong Xu, Ya-Hui Zhang, Joshua Folk *et al.*, Chern insulators at integer and fractional filling in moiré pentalayer graphene, Phys. Rev. X **15**, 011045 (2025).
[18] Zhengguang Lu, Tonghang Han, Yuxuan Yao, Zach Hadjri, Jixiang Yang, Junseok Seo, Lihan Shi, Shenyong Ye, Kenji Watanabe, Takashi Taniguchi, and Long Ju, Extended quantum anomalous Hall states in graphene/hBN moiré superlattices, Nature (London) **637**, 1090 (2025).
[19] Junkai Dong, Taige Wang, Tianle Wang, Tomohiro Soejima, Michael P. Zaletel, Ashvin Vishwanath, and Daniel E. Parker, Anomalous Hall crystals in rhombohedral multilayer graphene. I. Interaction-driven Chern bands and fractional quantum Hall states at zero magnetic field, Phys. Rev. Lett. **133**, 206503 (2024).
[20] Boran Zhou, Hui Yang, and Ya-Hui Zhang, Fractional quantum anomalous Hall effect in rhombohedral multilayer graphene in the moiréless limit, Phys. Rev. Lett. **133**, 206504 (2024).
[21] Zhihuan Dong, Adarsh S. Patri, and T. Senthil, Theory of quantum anomalous Hall phases in pentalayer rhombohedral graphene moiré structures, Phys. Rev. Lett. **133**, 206502 (2024).
[22] Zhongqing Guo, Xin Lu, Bo Xie, and Jianpeng Liu, Fractional Chern insulator states in multilayer graphene moiré superlattices, Phys. Rev. B **110**, 075109 (2024).
[23] Yves H. Kwan, Jiabin Yu, Jonah Herzog-Arbeitman, Dmitri K. Efetov, Nicolas Regnault, and B. Andrei Bernevig, Moiré'e fractional Chern insulators III: Hartree-Fock phase diagram, magic angle regime for Chern insulator states, the role of the moiré potential and goldstone gaps in rhombohedral graphene superlattices, Phys. Rev. B **112**, 075109 (2025).
[24] Tomohiro Soejima, Junkai Dong, Taige Wang, Tianle Wang, Michael P. Zaletel, Ashvin Vishwanath, and Daniel E. Parker, Anomalous Hall crystals in rhombohedral multilayer graphene. II. General mechanism and a minimal model, Phys. Rev. B **110**, 205124 (2024).
[25] Zhihuan Dong, Adarsh S. Patri, and T. Senthil, Stability of anomalous Hall crystals in multilayer rhombohedral graphene, Phys. Rev. B **110**, 205130 (2024).
[26] Jiabin Yu, Jonah Herzog-Arbeitman, Yves H. Kwan, Nicolas Regnault, and B. Andrei Bernevig, Moiré fractional Chern insulators IV: Fluctuation-driven collapse of fcis in multi-band exact diagonalization calculations on rhombohedral graphene, Phys. Rev. B **112**, 075110 (2025).
[27] Boran Zhou and Ya-Hui Zhang, New classes of quantum anomalous Hall crystals in multilayer graphene, Phys. Rev. Lett. **135**, 036501 (2025).
[28] Valentin Crépel and Jennifer Cano, Efficient prediction of superlattice and anomalous miniband topology from quantum geometry, Phys. Rev. X **15**, 011004 (2025).
[29] B. Andrei Bernevig and Yves H. Kwan, "Berry trashcan" model of interacting electrons in rhombohedral graphene, arXiv:2503.09692.
[30] Yongxin Zeng, Daniele Guerci, Valentin Crépel, Andrew J. Millis, and Jennifer Cano, Sublattice structure and topology in spontaneously crystallized electronic states, Phys. Rev. Lett. **132**, 236601 (2024).
[31] Tixuan Tan and Trithep Devakul, Parent berry curvature and the ideal anomalous Hall crystal, Phys. Rev. X **14**, 041040 (2024).
[32] Tixuan Tan, Julian May-Mann, and Trithep Devakul, Wavefunction approach to the fractional anomalous Hall crystal, arXiv:2409.06775.
[33] Félix Desrochers, Mark R. Hirsbrunner, Joe Huxford, Adarsh S. Patri, T. Senthil, and Yong Baek Kim, Elastic response and instabilities of anomalous Hall crystals, arXiv:2503.08784.
[34] Note that 1 Ry differs from the other standard measure of energy, a Hartree, by a factor of 2.
[35] See Supplemental Material at http://link.aps.org/supplemental/10.1103/x53d-12s6 for the construction of the model, modeling details, review of Ewald summation and Madelung energy, Hartree-Fock procedure, Berry curvature and band structure of the crystalline states, finite-size scaling of the energy, and semiclassical analysis for the Wigner crystal phase transition, which includes Refs. [36–40].
[36] Sandeep Joy and Brian Skinner, Wigner crystallization in bernal bilayer graphene, arXiv:2310.07751.
[37] Masaaki Kawata and Masuhiro Mikami, Rapid calculation of two-dimensional Ewald summation, Chem. Phys. Lett. **340**, 157 (2001).
[38] D. E. Parry, The electrostatic potential in the surface region of an ionic crystal, Surf. Sci. **49**, 433 (1975).
[39] R. J. Hunt, M. Szyniszewski, G. I. Prayogo, R. Maezono, and N. D. Drummond, Quantum Monte Carlo calculations of energy gaps from first principles, Phys. Rev. B **98**, 075122 (2018).
[40] Hannah M. Price, Tomoki Ozawa, Nigel R. Cooper, and Iacopo Carusotto, Artificial magnetic fields in momentum space in spin-orbit-coupled systems, Phys. Rev. A **91**, 033606 (2015).

[41] B. Andrei Bernevig, Taylor L. Hughes, and Shou-Cheng Zhang, Quantum spin Hall effect and topological phase transition in HgTe quantum wells, Science **314**, 1757 (2006).
[42] Yichen Hu, Jörn W. F. Venderbos, and C. L. Kane, Fractional excitonic insulator, Phys. Rev. Lett. **121**, 126601 (2018).
[43] This nonuniform Berry curvature is in contrast to the uniform Berry curvature of the model studied in Ref. [31]. In contrast, the λ-jellium model always has two-component spinors with Berry curvature concentrated around $\boldsymbol{k} = 0$.
[44] Jie Wang, Jennifer Cano, Andrew J. Millis, Zhao Liu, and Bo Yang, Exact Landau level description of geometry and interaction in a flatband, Phys. Rev. Lett. **127**, 246403 (2021).
[45] Patrick J. Ledwith, Ashvin Vishwanath, and Daniel E. Parker, Vortexability: A unifying criterion for ideal fractional Chern insulators, Phys. Rev. B **108**, 205144 (2023).
[46] Lynn Bonsall and A. A. Maradudin, Some static and dynamical properties of a two-dimensional Wigner crystal, Phys. Rev. B **15**, 1959 (1977).
[47] G. Meissner, H. Namaizawa, and M. Voss, Stability and image-potential-induced screening of electron vibrational excitations in a three-layer structure, Phys. Rev. B **13**, 1370 (1976).
[48] Tsuneya Ando, Alan B. Fowler, and Frank Stern, Electronic properties of two-dimensional systems, Rev. Mod. Phys. **54**, 437 (1982).
[49] Hoi Chun Po, Symmetry indicators of band topology, J. Phys. Condens. Matter **32**, 263001 (2020).
[50] Junkai Dong, Ophelia Evelyn Sommer, Tomohiro Soejima, Daniel E. Parker, and Ashvin Vishwanath, Phonons in electron crystals with Berry curvature, Proc. Natl. Acad. Sci. U.S.A. **122**, e2515532122 (2025).